BIOCHEMISTRY
including biophysical chemistry & molecular biology
Article

Biochemistry **2009,** *48,* 9891–9902 9891
DOI: 10.1021/bi9008853

Structural Insights into Glucan Phosphatase Dynamics Using Amide Hydrogen−Deuterium Exchange Mass Spectrometry[†]

Simon Hsu,[‡] Youngjun Kim,[§] Sheng Li,[‡] Eric S. Durrant,[‡] Rachel M. Pace,[∥] Virgil L. Woods, Jr.,*[,‡] and Matthew S. Gentry*[,∥,⊥]

[‡]*Department of Medicine, University of California at San Diego, La Jolla, California 92093-0601,* [§]*Department of Applied Biochemistry, Konkuk University, 322 Danwol-dong, Chungju-city, Chungbuk 380-701, Korea,* [∥]*Department of Molecular and Cellular Biochemistry, and* [⊥]*Center for Structural Biology, University of Kentucky, Lexington, Kentucky 40536*

Received May 26, 2009; Revised Manuscript Received August 14, 2009

ABSTRACT: Laforin and starch excess 4 (SEX4) are founding members of a class of phosphatases that dephosphorylate phosphoglucans. Each protein contains a carbohydrate binding module (CBM) and a dual-specificity phosphatase (DSP) domain. The gene encoding laforin is mutated in a fatal neurodegenerative disease called Lafora disease (LD). In the absence of laforin function, insoluble glucans that are hyperphosphorylated and exhibit sparse branching accumulate. It is hypothesized that these accumulations trigger the neurodegeneration and premature death of LD patients. We recently demonstrated that laforin removes phosphate from phosphoglucans and hypothesized that this function inhibits insoluble glucan accumulation. Loss of SEX4 function in plants yields a similar cellular phenotype; an excess amount of insoluble, hyperphosphorylated glucans accumulates in cells. While multiple groups have shown that these phosphatases dephosphorylate phosphoglucans, there is no structure of a glucan phosphatase and little is known about the mechanism whereby they perform this action. We utilized hydrogen−deuterium exchange mass spectrometry (DXMS) and structural modeling to probe the conformational and structural dynamics of the glucan phosphatase SEX4. We found that the enzyme does not undergo a global conformational change upon glucan binding but instead undergoes minimal rearrangement upon binding. The CBM has improved protection from deuteration when bound to glucans, confirming its role in glucan binding. More interestingly, we identified structural components of the DSP that also have improved protection from deuteration upon glucan addition. To determine the position of these regions, we generated a homology model of the SEX4 DSP. The homology model shows that all of these regions are adjacent to the DSP active site. Therefore, our results suggest that these regions of the DSP participate in the presentation of the phosphoglucan to the active site and provide the first structural analysis and mode of action of this unique class of phosphatases.

The major storage carbohydrates or glucans in plants and animals are starch and glycogen, respectively. Both polymers are composed of α-1,4-glycosidic linkages between glucose residues with branches attached by α-1,6-glycosidic linkages. The major differences between the two polymers are that glycogen exhibits consistent branching every 12−14 glucose monomers and amylopectin, the major component of starch, exhibits clustered branching every 12−20 glucose monomers and clustered regions with no branching. These differences in branching patterns largely account for the fact that glycogen is water-soluble and starch is insoluble.

Lafora disease (LD,[1] OMIM #254780) is an autosomal recessive neurodegenerative disease that results in epilepsy and death around age 30 (*1*, *2*). A hallmark of LD is the accumulation of insoluble glucans called Lafora bodies (LBs) (*3*, *4*). Glycogen, the normal energy storage glucan in metazoans, is water-soluble, regularly branched, and sparsely phosphorylated. Alternatively, LBs are sparsely branched, hyperphosphorylated glucans that are water-insoluble and closely resemble amylopectin, the major component of plant starch (*5*−*7*). Mutations in the gene encoding laforin result in LD (*8*, *9*). Laforin is a bimodular protein composed of a carbohydrate binding module (CBM) followed by a dual-specificity phosphatase (DSP) domain (*8*−*10*). We recently demonstrated that laforin has the unique activity of dephosphorylating phosphoglucans (*11*, *12*). Additionally, laforin is the only phosphatase in vertebrate genomes with a CBM

[†]This work was supported by National Institutes of Health (NIH) Grants 5R00NS061803 and 5P20RR0202171 and University of Kentucky College of Medicine startup funds (to M.S.G.), Korea Research Foundation Grant KRF-2008-331-E00031 (to Y.K.), and the Innovative Technologies for the Molecular Analysis of Cancer (IMAT) program [CA099835, and CA118595 (V.L.W.)], NIH Grants AI076961, AI081982, AI2008031, AI072106, AI068730, GM037684, GM020501, and GM066170 (V.L.W.), and a Discovery Grant (UC10591) from the University of California IUCRP Program, BiogenIDEC corporate sponsor (to V.L.W.).

*To whom correspondence should be addressed. M.S.G.: 741 S. Limestone, BBSRB, B177, Lexington, KY 40536-0509; telephone, (859) 323-8482; fax, (859) 323-5505; e-mail, matthew.gentry@uky.edu. V.L.W.: telephone, (858) 534-2180; fax, (858) 534-2606; e-mail, vwoods@ucsd.edu.

[1]Abbreviations: AMPKβ1, AMP-activated kinase targeting subunit β1; CBM, carbohydrate binding module; cTP, chloroplast targeting peptide; DSP, dual-specificity phosphatase; DTT, dithiothreitol; DXMS, hydrogen−deuterium exchange mass spectrometry; GuHCl, guanidine hydrochloride; GWD, glucan water dikinase; LD, Lafora disease; LB, Lafora body; MTMR2, myotubularin-related protein-2; p-NPP, *p*-nitrophenyl phosphate; PROMALS3D, profile multiple alignment with predicted local structure 3D; PTPs, protein tyrosine-specific phosphatases; PWD, phosphoglucan water dikinase; SEX4, starch excess 4; VHR, vaccinia virus H1-related.

Published on Web 09/15/2009

and, as such, the only phosphatase predicted to possess this activity. Recent work from our lab, and others, has suggested that laforin dephosphorylates nascent glucans during glycogen metabolism to inhibit LB formation, but the mechanism of this action and the details of this proposed pathway are still being elucidated (*11*−*17*).

The *starch excess 4* (*SEX4*) gene is conserved in all members of Archaeplastida/Kingdom Plantae (*18*). Mutations in *SEX4* result in excess starch accumulation in *Arabidopsis* cells (*19*, *20*). This cellular phenotype is similar to the cellular phenotype observed in LD patients, i.e., excess insoluble glucan accumulation. The SEX4 protein is composed of a chloroplast Targeting Peptide (cTP), followed by a DSP domain, and then a CBM (*19*, *21*). Similar to laforin, SEX4 also binds and dephosphorylates phosphoglucans, and we recently demonstrated that laforin can functionally replace SEX4 (*11*).

In plants, unlike in vertebrates, significant progress has been made in understanding phosphoglucan metabolism as a means of storing and accessing energy caches (*22*−*25*). The emerging theme for starch breakdown in *Arabidopsis* is as follows. Glucose monomers on the surface of starch are phosphorylated at the C6 and C3 positions by glucan water dikinase (GWD) and phosphoglucan water dikinase (PWD), respectively. β-Amylase cleaves glucose polymers and releases maltose. The glucan phosphatase SEX4 releases phosphates, and the debranching enzyme isoamylase hydrolyzes branch points while α-amylase releases oligosaccharides (*22*−*26*). In the absence of SEX4 activity, β-amylase activity is inhibited and α-amylase releases phospho-oligosaccharides (*22*). Thus, there is a coordinated phosphorylation and dephosphorylation of the glucan that is necessary for proper starch breakdown.

Little is known regarding the structural dynamics of glucan phosphatases, i.e., how the two domains interact both before and during glucan binding. In addition, the structural properties that allow glucan phosphatases to accommodate a phosphoglucan in their active site, rather than the typical phosphopeptide, are entirely unknown. Therefore, we set out to determine if conformational changes occur upon glucan binding and to identify the regions of SEX4 that interact with phosphoglucans, being particularly interested in if or how the phosphatase domain of SEX4 interacts with phosphoglucans. Deuterium exchange techniques have been employed to probe protein structure for more than 50 years (*27*, *28*). In more recent years, deuterium exchange has been coupled with pepsin proteolysis, HPLC separation, and mass spectrometry and further developed into a powerful technique known as hydrogen−deuterium exchange mass spectrometry (DXMS) (*29*−*31*).

Since there is no available structure of a glucan phosphatase and only limited structural information about glucan phosphatases, we probed the conformational and dynamic changes of the glucan phosphatase SEX4 upon glucan binding using DXMS. Once glucan bound, we observed a decrease in the level of deuteration of multiple peptides but did not observe any substantial increases in the level of deuteration. These results indicate that SEX4 does not undergo a large-scale conformational change when it binds glucans. We observed decreases in the level of deuteration in both the CBM and DSP domain. We found that upon glucan binding the proposed regions of the CBM that bind the glucan are more resistant to deuteration. This result is as expected, since the glucan would inhibit deuteration to this region upon binding. More surprisingly, we found that bound glucan also protected specific regions of the DSP domain from deuteration. A homology model of the SEX4 DSP revealed that each of these regions is adjacent the SEX4 DSP active site and suggests that these regions participate in presentation of phosphoglucan to the SEX4 active site. Thus, we present the first data that elucidate the mechanistic action of a glucan phosphatase.

EXPERIMENTAL PROCEDURES

Protein Expression, Purification, and Western Analysis. Δ81-SEX4, Δ52-SEX4, and all mutants were expressed with a C-terminal His_6 tag in *Escherichia coli* BL21(DE3) CodonPlus cells (Stratagene). Most of the fusion proteins were expressed and purified from soluble bacterial extracts using Ni^{2+}-agarose affinity chromatography as previously described (*32*). The Δ81-SEX4-C198S used in DXMS studies was purified using a Profinia IMAC column (Bio-Rad) with a Profinia protein purification system (Bio-Rad). Monomeric Δ81-SEX4-C198S from the Profinia system was purified to near homogeneity using a HiLoad 16/60 Superdex 200 size exclusion column (GE Healthcare) and concentrated to 10 mg/mL. Purifications were performed in 20 mM Tris-HCl, 100 mM NaCl, 15 mM imidazole, and 2 mM dithiothreitol (DTT) (pH 7.2). Western analysis was performed on His-tagged proteins using mouse α-6HIS (NeuroMab) and goat α-mouse HRP (Zymed).

Optimization of Pepsin Digestion of SEX4. Target protein digestion by pepsin is a requisite step prior to DXMS experiments. In the optimization of this process, the total number of peptides produced from pepsin digestion was evaluated under several different conditions, including concentrations of denaturant. For each sample test, 5 μL of Δ81-SEX4-C198S was diluted in 15 μL of 100 mM NaCl, 2 mM DTT, and 7.8 mM Tris (pH 7.1) (on ice), representing the dilution of the protein into D_2O-based buffers in deuterium exchange experiments. The sample was then diluted with 30 μL of a cold quench solution (0 °C) of 0.8% formic acid, 16.6% glycerol, and guanidine hydrochloride (GuHCl) at final concentrations of 0.05, 0.5, 1.0, 2.0, or 4.0 M. This quenching step represented the reduction of the level of hydrogen−deuterium exchange with a decrease in pH to 2.2−2.5 in addition to denaturing the protein prior to pepsin proteolysis with GuHCl and acidic conditions. The quenching−denaturation process was allowed to proceed on ice for 30 s, after which the sample was frozen by being submersed in dry ice. The frozen sample was stored at −80 °C until it was transferred to the dry ice-containing sample basin of the cryogenic autosampler module of the DXMS apparatus. Procedures for pepsin digestion for DXMS have been described previously (*33*−*36*). Briefly, the sample was thawed at 0 °C and injected and pumped through a porcine pepsin-immobilized column (Sigma), and the protease-generated peptides were collected on a C18 HPLC column (Vydac). The column effluent was analyzed on an LCQ Classic (Thermo Finnigan, Inc.) electrospray ion trap-type mass spectrometer and an electrospray Q-TOF mass spectrometer (Micromass). Determination of pepsin-generated peptide sequences from the resulting MS/MS data sets was facilitated through the use of SEQUEST (Thermo Finnigan, Inc.).

Hydrogen−Deuterium Exchange. DXMS experiments were performed as previously described (*33*−*37*). Δ81-SEX4-C198S samples were prepared with three states of hydrogen−deuterium exchange in each deuterium exchange experiment, consisting of nondeuterated (ND), deuterated, and fully deuterated (FD). The nondeuterated sample was processed via

digestion optimization exactly as described in the previous paragraph. The FD sample represents the "maximum" hydrogen−deuterium exchange for a certain time period, which in these experiments was a period of 24 h during which the samples were allowed to exchange at room temperature in D_2O buffer [1% (v/v) formic acid]. The deuterated samples represent different incubation times prior to the quenching of the exchange process. Briefly, a 5 μL solution of Δ81-SEX4-C198S (10 mg/mL) was diluted with 15 μL of ice-cold D_2O buffer [7.8 mM Tris-HCl and 100 mM NaCl (pH 7.1) with or without 5 mM β-cyclodextrin], samples were incubated at 0 °C for 10, 30, 100, 300, 1000, 3000, and 10000 s (166.67 min) and then mixed with 30 μL of quench solution [0.8% (v/v) formic acid, 0.08 M guanidine hydrochloride, and 16.6% (v/v) glycerol] with samples on ice for 30 s, and then samples were transferred to ice-cooled autosampler vials, frozen on dry ice, and stored at −80 °C. In amylopectin binding experiments, Δ81-SEX4-C198S was preincubated with 5 mg/mL amylopectin (Sigma) at room temperature for 30 min and then chilled to 0 °C. The pepsin digestion (16 s), chromatography, and the mass spectral acquisition proceeded as described in the digestion optimization section. This process is an automated system, such that the time between protein loading onto pepsin and mass spectral acquisition is constant (~7 min) for each sample. All of the samples for one protein were prepared and run on the same day. Each apo and amylopectin-bound DXMS experiment was performed a minimum of three times, and for each experiment, we prepared and analyzed samples in triplicate. The ribbon maps and graphs are the average percent deuteration with the standard deviation. Data processing and reduction of hydrogen−deuterium exchange experiments utilized specialized DXMS data reduction software (Sierra Analytics, Modesto, CA) (*17*, *25*, *26*). Corrections for back exchange were determined via the methods of Zhang and Smith (*38*)

$$\text{deuteration level } (\%) = \frac{m(P) - m(N)}{m(F) - m(N)} \times 100$$

where $m(P)$, $m(N)$, and $m(F)$ are the centroid value of the partially deuterated, nondeuterated, and fully deuterated peptide, respectively.

Homology Modeling of SEX4. HHpred search (*39*, *40*) and InterPro domain scan (*41*) were used to determine which available structure of a DSP domain was the best template for modeling the DSP domain of SEX4. The top four hits of each search were aligned with the DSP domain of SEX4 using PROfile Multiple Alignment with predicted Local Structure 3D (PROMALS3D) (*42*). These alignments served as inputs for the alignment mode of SWISS-MODEL in Swiss PDB viewer version 8.05 (*43*) for the generation of a homology model of the SEX4 DSP domain. Each homology model was analyzed visually and by Anolea, Gromos, and Verify3d (*44*−*46*). The model utilizing VHR (Protein Data Bank entry 1vhr) as the template was the best model.

RESULTS

Laforin and SEX4 are both composed of a carbohydrate binding module (CBM) and a dual-specificity phosphatase (DSP) domain (Figure 1A). In addition to these two domains, SEX4 also contains a chloroplast targeting peptide (cTP), to target it to the site of starch synthesis in plants. The CBM of laforin and SEX4 are 38% similar at the amino acid level (Figure 1B), and while they belong to different CBM families, CBM20 and CBM21,

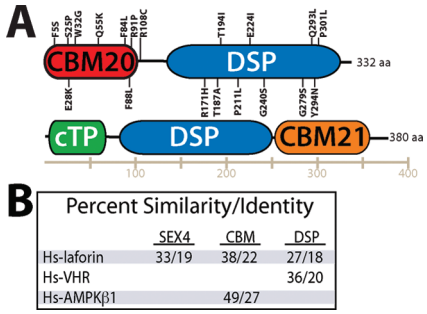

FIGURE 1: Laforin and SEX4 domain structure and similarity of SEX4 with other CBM and DSP domains. (A) Laforin is composed of a carbohydrate binding module, family 20 (CBM20), a linker region, and a dual-specificity phosphatase (DSP) domain. LD patient nonsense mutations are shown. SEX4 contains a chloroplast targeting peptide (cTP), a DSP, and a carbohydrate binding module, family 21 (CBM21). (B) Percent similarity and identity of full-length SEX4 and both domains compared with those of *Homo sapiens* laforin (Hs-laforin), VHR (Hs-VHR), and AMPKβ1 (Hs-AMPKβ1).

respectively, they belong to the same evolutionarily related CBM clan (*47*−*49*). AMP-activated kinase targeting subunit β1 (AMPKβ1) is also a member of this clan, shares 49% similarity with the SEX4 CBM, and is the closest homologue with a determined crystal structure and detailed knowledge of key residues that are necessary for glucan binding (*50*). The phosphatase domains of laforin and SEX4 are 33% similar (Figure 1B). A BLASTp search of the nonredundant GenBank human database with the SEX4 DSP identified laforin as the closest match (6×10^{-7}) and human vaccinia virus H1-related (VHR) phosphatase as the one of the closest matches with a determined structure (2×10^{-4}). The DSP of SEX4 and VHR are 36% similar at the amino acid level (Figure 1B). For these reasons, we utilized the structural information known about the CBM of AMPKβ1 and the DSP domain of VHR throughout our study.

Recombinant Expression, Purification, and Biochemical Characterization of Δ81-SEX4. We previously reported that full-length SEX4 is largely insoluble; however, deletion of the first 52 amino acids (Δ52-SEX4) yields a soluble protein (*11*). We also previously demonstrated that recombinant Δ52-SEX4 binds carbohydrates, utilizes the exogenous phosphatase substrate *p*-nitrophenyl phosphate (p-NPP), and has the unique activity of dephosphorylating phosphoglucans (*11*). This was the first extensive biochemical characterization of a glucan phosphatase that reported all three of these functions.

Truncation of the first 52 amino acids deletes most of the cTP of SEX4 (Figure 2A). However, the PTP fold does not begin until approximately residue 81, and we felt leaving residues 52−80 might interfere in our DXMS studies. Therefore, we generated Δ81-SEX4 to eliminate this entire region (Figure 2A). Before proceeding to DXMS studies, we first characterized Δ81-SEX4 to ensure it behaved like Δ52-SEX4. We found that Δ81-SEX4 has a lower specific activity than Δ52-SEX4 against p-NPP (Figure 2B). While Δ81-SEX4 has a lower activity against the exogenous substrate p-NPP, it liberates phosphate from amylopectin to a greater extent than Δ52-SEX4 (Figure 2C). Phosphatase activity by a DSP is dependent on a nucleophilic cysteine residue conserved in the DSP signature motif, H**C**xxGxxRS (*51*, *52*). Therefore, we mutated this residue and, as expected, found that activities against phosphoglucans and p-NPP are both dependent on the catalytic cysteine (Figure 2B,C). With respect to glucan binding, Δ81-SEX4 and Δ81-SEX4-C/S both bind amylopectin to similar degrees as previously observed for Δ52-SEX4 (Figure 2D) (*11*).

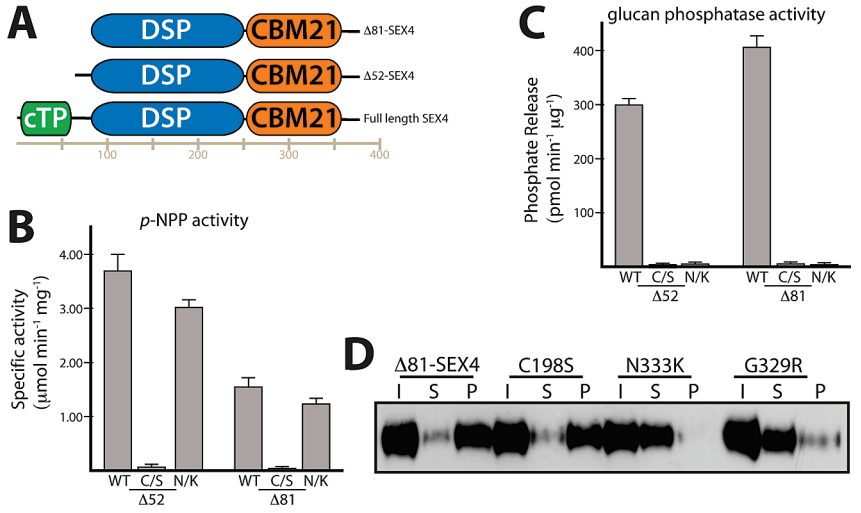

FIGURE 2: Biochemical characterization of SEX4 truncations. (A) Schematic of SEX4 recombinant proteins used in this study: full-length, amino-terminal truncation of 52 amino acids (Δ52-SEX4), and amino-terminal truncation of 81 amino acids (Δ81-SEX4). The schematic is to scale. (B) Specific activity of Δ52-SEX4 and Δ81-SEX4 against *p*-nitrophenyl phosphate (p-NPP): WT, wild-type; C/S, C198S; N/K, N333K. (C) Release of phosphate from amylopectin by malachite green assays using Δ52-SEX4 and Δ81-SEX4 and mutants as in panel B. Error bars indicate means ± the standard deviation. (D) Δ81-SEX4 recombinant histidine-tagged protein, input (I), was incubated with 5 mg/mL amylopectin; amylopectin was pelleted by ultracentrifugation, and proteins in the input (I), pellet (P), and supernatant (S) were visualized by Western analysis as described. Mutated residues are designated with an asterisk in Figure 4 and highlighted in Figure 5 of the Supporting Information.

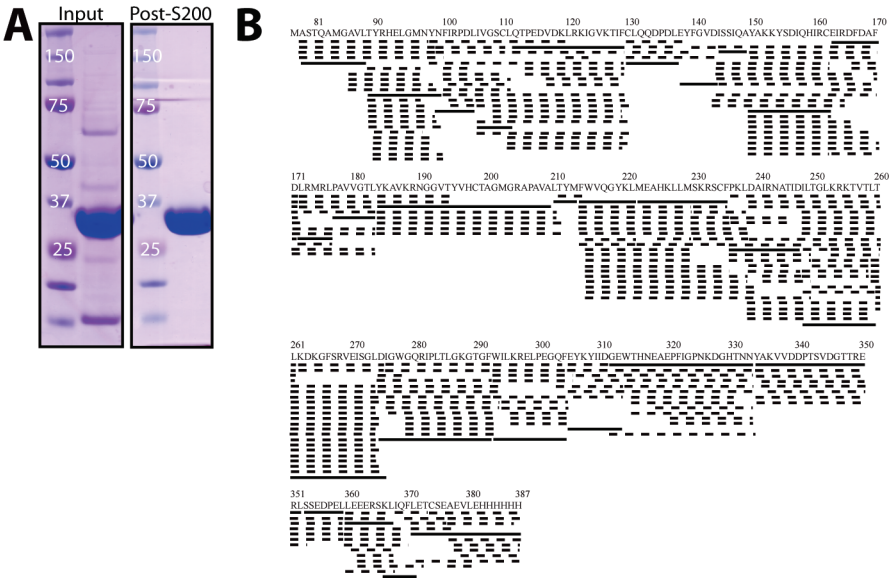

FIGURE 3: Purified recombinant protein and pepsin-digested coverage map. (A) Δ81-SEX4-His_6 was purified from *E. coli* supernatants using a Profinia IMAC cartridge. The eluate was then purified to near homogeneity by separation over a S200 gel filtration column. (B) Sequence coverage map of pepsin-digested peptides identified in the MS/MS experiments. A total of 264 peptides were detected. Solid lines indicate the 28 peptides utilized for our analysis, and dashed lines indicate peptides not used for our analysis. Numbers correspond to full-length SEX4 with amino acid 81 beginning with the first threonine in the sequence.

As previously mentioned, the CBM of AMPKβ1 is closely related to the CBM of SEX4, and the AMPKβ1 CBM is structurally well-defined. Polekhina and colleagues demonstrated which residues in the CBM of AMPKβ1 participate in glucan binding (*50*, *53*). On the basis of this work, we mutated residues predicted to participate in glucan binding of SEX4. As expected, these mutations abolished or greatly reduced the level of binding of glucan to Δ81-SEX4 (Figure 2D). We reported for Δ52-SEX4 that inhibition of glucan binding also inhibited glucan phosphatase activity (*11*). As for Δ52-SEX4, mutation of the glucan binding residue in Δ81-SEX4 also greatly reduced its glucan phosphatase activity but did not affect its p-NPP activity (Figure 2B,C). Cumulatively, these data show that Δ81-SEX4 behaves in a similar manner as previously reported for Δ52-SEX4 and suggest that partial truncation of the cTP (Δ52-SEX4) may slightly inhibit the glucan phosphatase activity of SEX4.

Pepsin Fragmentation and Peptide Identification of Δ81-SEX4-C/S. Mutation of a DSP nucleophilic cysteine to a serine inhibits substrate dephosphorylation but allows the phosphatase to correctly position the substrate in the active site cleft (*54*, *55*). In addition, the Cys/Ser mutant binds substrates with affinities similar to that of the wild-type enzyme (*56*−*58*). Therefore, we utilized the catalytically inactive Δ81-SEX4-C/S form in our

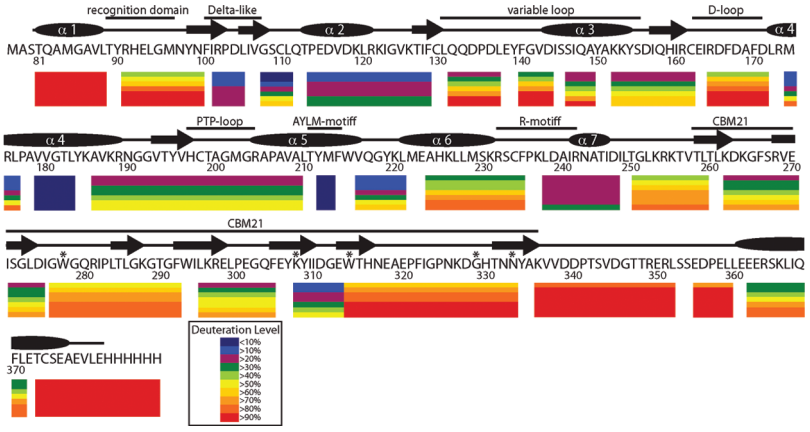

FIGURE 4: H−D exchange results of glucan-free Δ81-SEX4. The deuteration level of glucan-free Δ81-SEX4 (apo-Δ81-SEX4) is shown with the lowest deuteration levels in blue to highest deuteration levels in red, as indicated by the inset. Each row represents the peptide we analyzed from Figure 3B. Each bar represents the level of deuteration at one of the seven time points from 10 to 10000 s (166 min). The DSP domain extends from amino acid 81 to 249, and important regions are labeled appropriately. The CBM extends from amino acid 256 to 337. Residues predicted to be necessary for glucan binding are denoted with asterisks. The predicted secondary structure of SEX4 is designated above the amino acids. α-Helices in the DSP domain are labeled per standard nomenclature. Amino acid numbers refer to the amino acid positions in full-length SEX4. Deuterons from the first two amino acids of each peptide are lacking due to the fact that the first amino acid of each peptide lacks an amide hydrogen and the second amide hydrogen exchanges too rapidly to retain deuterons during processing. Therefore, the exchange data are lacking for the first two amino acids of each peptide in this figure. There is no gap between amino acids 313 and 314 because we analyzed overlapping peptides in this region to have exchange data covering W314 since W314 is proposed to play an integral part in glucan binding.

DXMS analysis and purified it to >95% homogeneity (Figure 3A and Figure 1 of the Supporting Information).

We first optimized the pepsin digestion and HPLC separation conditions of Δ81-SEX4-C/S so that we produced fragments of the appropriate size and distribution for exchange analysis. We optimized digestion by diluting nondeuterated Δ81-SEX4-C/S with 1.5 parts of the quench solution and then exposing the sample to immobilized pepsin for 16 s. These conditions resulted in the production and identification of 264 probe peptides covering 100% of the 307 amino acids of Δ81-SEX4-C/S (Figure 3B). Of these 264 peptides, we chose 28 peptides that covered the entire sequence to monitor in subsequent experiments.

H−D Exchange of Apo-Δ81-SEX4-C/S. We began our H−D exchange experiments using Δ81-SEX4-C/S in the absence of glucan (apo-Δ81-SEX4-C/S). We incubated Δ81-SEX4-C/S in D_2O for 10−10000 s (166.67 min), quenched the reactions by rapidly lowering the pH and temperature, digested the sample with pepsin, separated the peptides by HPLC, and analyzed the in-exchange rate of deuterium by electrospray ionization mass spectrometry.

Combining the H−D exchange data with the peptide map allows one to assess the level of deuteration for specific regions of the protein. In apo-Δ81-SEX4-C/S, the regions of the DSP domain that were highly accessible to solvent, defined as more than 50% deuterated after 300 s in D_2O, are regions predicted to be between β-sheets and α-helices in SEX4 (Figure 4) and known to be in loops and turns in phosphatase crystal structures (reviewed in refs *51* and *59*−*61*). The only peptide that did not behave in this manner was peptide 79−88, the amino-terminal peptide. Peptide 79−88 is predicted to be an α-helix but exhibited >90% deuteration at the earliest time point. This result is likely due to the fact that we truncated the first 80 amino acids of SEX4 and disrupted this predicted helix.

Within the DSP domain, the recognition domain, D-loop, PTP-loop, and the first half of the variable loop (amino acids 130−143) were all highly solvent accessible regions (Figure 4). Within the CBM, two regions that contain residues known to coordinate glucan binding, 275−292 and 312−333, were highly accessible as were residues 334−360 and the carboxy-terminal tail (Figure 4).

The highly accessible portions of the DSP domain fall within the active site (PTP-loop) and regions known to coordinate substrate presentation to the active site in other dual-specificity phosphatases (i.e., the D-loop, recognition domain, and variable loop) (*59*−*61*). Within the CBM, four of the five residues (W278, W314, G329, and N333) known to coordinate glucan binding are within regions that are highly solvent accessible. The high levels of deuteration in these portions of the DSP domain and CBM are predicted to be in exposed loops and/or bind the phosphoglucan.

Percent Change in the Level of H−D Exchange of Apo versus Amylopectin-Bound Δ81-SEX4-C/S. We then performed the same experiment as described above for Apo-Δ81-SEX4-C/S using Δ81-SEX4-C/S in the presence of the phosphoglucan amylopectin. Figure 5 shows the spectra for one peptide (residues 312−333) from the CBM prior to exposure to D_2O (no D_2O), after exposure to D_2O in the absence of amylopectin (Apo), and after exposure to D_2O in the presence of amylopectin (+Amylopectin). Incorporation of deuterium is evident from the increase in mass and complexity of the peaks as a function of deuteration time (Figure 5A,B). When Δ81-SEX4-C/S binds amylopectin, the spectra undergo a prominent leftward shift on the *m*/*z* axis, indicating a uniform decrease in the level of deuteration when bound to amylopectin. This shift is in sharp contrast to spectra for the apo form (Figure 5B) and the fully deuterated peptide (Figure 5D).

We investigated each of the 28 peptides from Figure 3 of Δ81-SEX4-C/S, apo and amylopectin-bound, in a manner similar to that described in the legend of Figure 5 to identify peptides that underwent increased, decreased, or no change in the level of H−D exchange upon substrate binding. To compare the deuteration changes in apo versus amylopectin-bound SEX4, we compared the percentage of deuteration in each peptide in the absence and presence of amylopectin. We identified 14 peptides that displayed a >10% change in their percent deuteration in the presence of amylopectin during the 10000 s experiment. For these

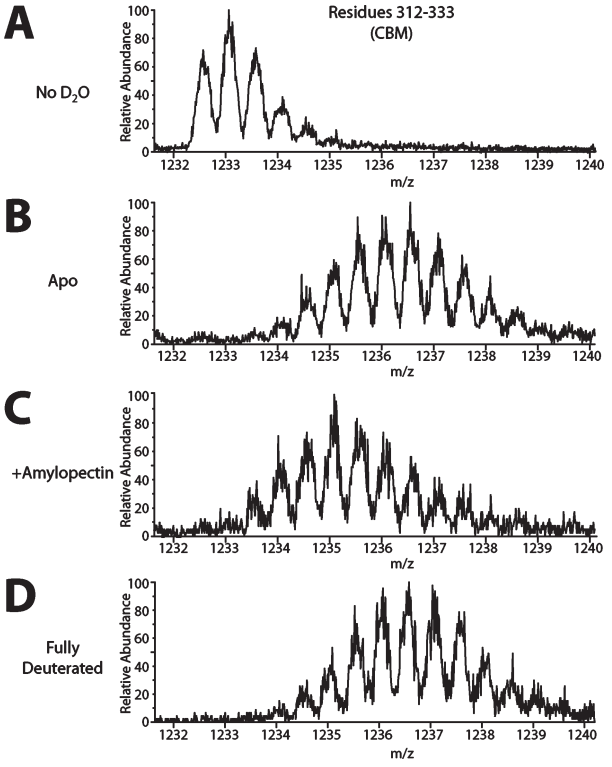

FIGURE 5: Mass spectra of pepsin-treated Δ81-SEX4 residues 312−333. (A) Mass spectra of a peptide covering residues 312−333, within the CBM, prior to exposure to D_2O. (B) Mass spectra of the same peptide as in panel A, but after it had been exposed to D_2O for 3000 s in the absence of amylopectin (Apo). Note the increase in complexity and mass compared to those in panel A. (C) Mass spectra of the same peptide as in panels A and B, but after it had been exposed to D_2O for 3000 s in the presence of amylopectin (+Amylopectin). Note the shift to a lower *m*/*z* ratio observed with amylopectin binding. (D) Mass spectra of the same peptide in panels A−C, but after it had been fully deuterated.

14 peptides, we did not observe any increases in the level of deuteration of >10%. Instead, all of the changes in percent deuteration were decreases. In the DSP domain, we identified eight peptides of 17 total that exhibited a considerable decrease (>10% decrease) in the level of deuteration in the presence of the glucan (Figure 6 and Figure 2 of the Supporting Information). In the CBM, we identified six peptides of eight total that exhibited a substantial decrease in their level of deuteration (Figure 7 and Figure 3 of the Supporting Information). We did not observe a change of >10% in percent deuteration in the peptides outside of these two domains (Figures 2 and 3 of the Supporting Information).

To determine the position of these peptides within SEX4, we overlaid the H−D exchange rates onto the peptides that were analyzed by mass spectrometry (Figure 4 and Figure 4 of the Supporting Information) and graphed the maximum percent change as a positive (increase) or negative (decrease) change in the level of deuteration (Figure 8A). Since we observed no increase in the level of deuteration of >10%, the percent changes shown in Figure 8A are percent decreases.

Within the CBM, peptides containing residues known to coordinate glucan binding all experienced a decreased level of H−D exchange upon addition of glucan (Figure 8A, arrows). Poekhlina et al. showed that these residues in the CBM21 domain of AMPKβ1 subunit all contact the glucan (*50*, *53*). In addition, we demonstrated that mutation of these residues in Δ81-SEX4 and Δ52-SEX4 reduces or abolishes glucan binding (Figure 2D and ref *11*). Therefore, the decrease in the level of H−D exchange of these residues suggests that they are performing the same function in Δ81-SEX4-C/S, i.e., binding the glucan. In addition to these regions of the CBM, residues 260−275 and 293−304 also undergo >20 and >30% decreases, respectively, in their level of deuteration upon amylopectin binding (Figures 7A and 8A). While residues in this region of the CBM are not known to be necessary for glucan binding, these peptides encompass β-sheets in the AMPKβ1 structure that are in the proximity of the substrate and are predicted to be located in analogous β-sheets in the SEX4 CBM (Figure 5 of the Supporting Information) (*50*). Thus, our data suggest these regions in SEX4 are in contact with the glucan.

While the H−D exchange data from the CBM confirm known aspects of CBM−glucan binding, the exchange data from the DSP domain are most insightful. The four regions that coordinate presentation of the substrate to the active site of phosphatases are the recognition domain (residues 89−99), the variable loop (residues 130−161), the D-loop (residues 163−171), and the PTP-loop (residues 196−204) (*59*). Strikingly, these regions all undergo a dramatic decrease in their level of H−D exchange upon glucan binding (Figures 6 and 8A). Since we did not observe any substantial increases in the level of deuteration, these data strongly suggest an extensive interaction between these regions and the glucan and suggest that they are presenting the phosphoglucan to the active site. The interaction with the glucan then provides protection from deuteration for these regions.

In addition to peptides covering the four DSP regions mentioned above, we also observed a significant decrease in the level of deuteration in peptides 106−111 and 172−176 (Figure 6). Peptide 106−111 is predicted to be in a loop region between the δ-like domain and variable loop (Figure 4). Peptide 172−176 is within α-helix 4 of the DSP just prior to the PTP-loop (Figure 4). These regions have not been identified as playing a role in DSP substrate binding; however, to the best of our knowledge, whether analogous regions play a role in substrate binding in other DSPs has not been investigated. Thus, it is entirely possible that these two regions interact with the phosphoglucan, and as we discuss in subsequent sections, our data suggest that they are in a position to do so.

Since amylopectin is a heterogeneous polymer, we decided to perform a similar set of experiments using the homogeneous, seven-ring, cyclic oligosaccharide β-cyclodextrin. These experiments also identified the peptides within the CBM that contain the five known residues that coordinate glucan binding and amino acids 261−275 as regions protected from H−D exchange (Figure 8B). The largest change within the CBM was in peptide 305−313, yielding an approximate 20% greater decrease compared to that of amylopectin (Figure 8). On the basis of the crystal structure of the AMPKβ1 CBM (the closest CBM homologue with a determined structure), peptide 305−313 of SEX4 contains a glycine (G329) and aspargine (N333) that are predicted to make direct contact with β-cyclodextrin. Since β-cyclodextrin is much more homogeneous than amylopectin, the 20% greater decrease is likely the result of a higher percentage of β-cyclodextrin making contact with these residues and/or making more extensive contact with them.

The results for the DSP domain in the presence of β-cyclodextrin were not as dramatic as those observed with amylopectin, but β-cyclodextrin showed a pattern of protection similar to that of amylopectin, with the highest degree of protection in the variable

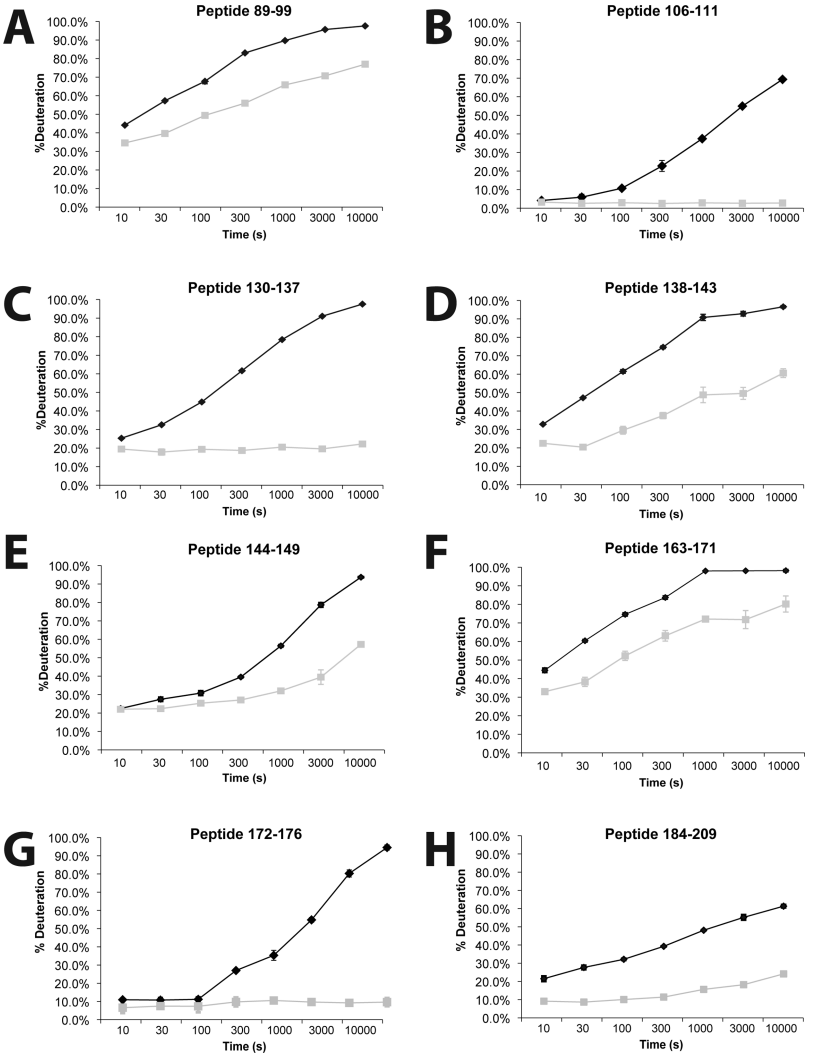

FIGURE 6: DSP domain peptides that exhibited a change in deuterium incorporation for apo vs amylopectin-bound peptides. Time-dependent incorporation in SEX4 peptides (A) $Thr^{89}-Asn^{99}$, (B) $Ile^{106}-Leu^{111}$, (C) $Cys^{130}-Leu^{137}$, (D) $Glu^{138}-Asp^{143}$, (E) $Ile^{144}-Ala^{149}$, (F) $Glu^{163}-Asp^{171}$, (G) $Leu^{172}-Leu^{176}$, and (H) $Tyr^{184}-Ala^{209}$. Data shown as black diamonds and gray squares represent percentages of deuterium incorporation into apo and amylopectin-bound Δ81-SEX4-C/S, respectively, at multiple time points. The *x*-axis has a log scale.

loop (Figure 8B). This less robust result is likely due to the markedly smaller size of β-cyclodextrin compared to amylopectin. Cumulatively, these data strongly support our previous finding that SEX4 is a glucan phosphatase and yield insights into the mechanistic action of this activity.

Modeled Analysis of the SEX4 DSP Domain. To better interpret the predicted changes in the SEX4 DSP domain upon glucan binding, we generated a homology model of this region. As previously mentioned, a BLASTp search of the SEX4 DSP identifies laforin as the closest match (6×10^{-7}) and VHR as one of the closest matches with a determined structure (2×10^{-4}). In addition, the DSP of SEX4 and VHR are 36% similar at the amino acid level (Figure 1B). To identify the most appropriate crystal structure to utilize in our modeling efforts, we analyzed the sequence of the SEX4 DSP domain using HHpred search (*39*, *40*) and InterPro domain scan (*41*), both of which query alignment and structural databases, such as Pfam, SMART, PDB, CDD, and HMMTigr, using hidden Markov models. InterPro domain scan identified human VHR as the highest hit (3.3×10^{-37}), and HHpred identified VHR as one of the highest hits (7.2×10^{-37}). To confirm these results, we compared the predicted secondary structure of the SEX4 DSP domain with the known secondary structure of human VHR. The DSP domains of SEX4 and VHR share very similar predicted secondary structure (Figure 9A).

Because no crystal structure is available for a glucan phosphatase, we utilized the results given above to generate a homology model of the SEX4 DSP using the SWISS-MODEL function in Swiss PDB viewer (*43*). We first generated a sequence alignment of the DSP domains of SEX4 and VHR using PROfile Multiple Alignment with predicted Local Structure 3D (PROMALS3D), which utilizes primary, predicted secondary, and available tertiary information to align sequences (*42*). We then utilized the crystal structure of VHR to generate a homology model of the DSP domain of SEX4.

To gain insight into the spatial arrangement of our DXMS results, we overlaid the percent change in deuteration onto the structural model (Figure 9B). The regions of the SEX4 DSP that undergo a dramatic decrease in their level of deuteration upon glucan binding are the D-loop, the recognition domain, the variable loop, the PTP-loop, peptide 106−111, and peptide 172−176 (Figure 9B). The D-loop contains the aspartate that functions as the general acid−base catalyst in the dephosphorylation reaction and thus makes direct contact with the phosphorylated substrate (*52*). Saper and colleagues originally

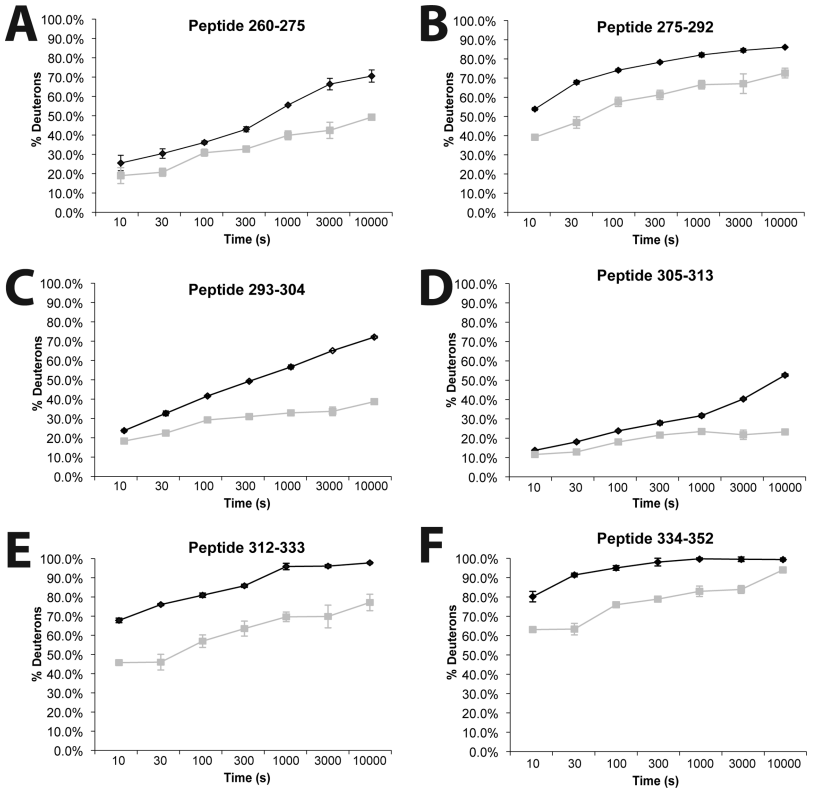

FIGURE 7: CBM peptides that exhibited a change in deuterium incorporation for apo vs amylopectin-bound peptides. Time-dependent incorporation in SEX4 peptides (A) $Thr^{260}-Asp^{275}$, (B) $Asp^{275}-Phe^{292}$, (C) $Trp^{293}-Phe^{304}$, (D) $Glu^{305}-Gly^{313}$, (E) $Asp^{312}-Asn^{333}$, and (F) $Tyr^{334}-Leu^{352}$. Data shown as black diamonds and gray squares represent percentages of deuterium incorporation into apo and amylopectin-bound Δ81-SEX4-C/S, respectively, at multiple time points. The *x*-axis has a log scale.

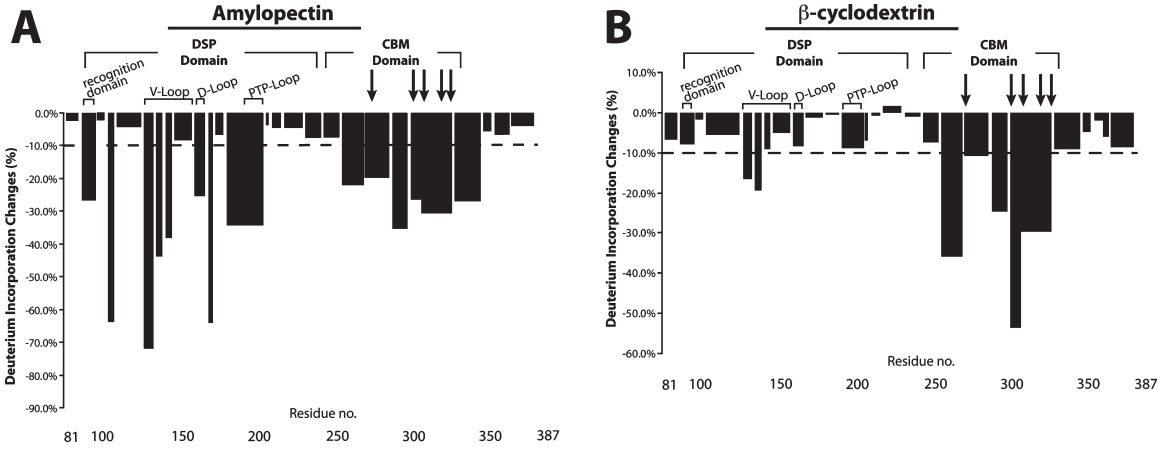

FIGURE 8: Maximal percent decreases in deuteration upon substrate binding. (A) Bar graph depicting the maximal percent decreases in deuteration between apo-Δ81-SEX4 and amylopectin-bound Δ81-SEX4. The different regions of the DSP domain are delineated at the top of the graph, and arrows signify the positions of residues within the CBM necessary for glucan binding. The residue numbers at the bottom refer to amino acid numbers of full-length SEX4. (B) Like panel A, with the exception that the comparison is between apo-Δ81-SEX4 and Δ81-SEX4 in the presence of *β*-cyclodextrin. In both panels A and B, the dotted line designates a $< 10\%$ decrease. Note that the scales are slightly different in panels A and B.

demonstrated that the recognition domain contributes to the depth of the active site and that it is also involved in substrate binding, aspects seen in other phosphatase structures as well (*52*, *55*, *62*, *63*). The variable loop assists in orienting the active site arginine to interact with the phosphate of the substrate and is in the proximity of the substrate (*52*, *59*). Within the PTP-loop, multiple residues participate in presenting the phospho-substrate to the active site and/or are involved in forming a phosphoenzyme intermediate with the substrate (*51*, *52*, *59*). Our homology model predicts that peptides 106−111 and 172−176 are positioned close to and on opposite sides of the active site. Thus, all of the regions of the DSP domain that undergo a dramatic decrease in the level of deuteration are the four regions that are involved in presenting the phosphosubstrate to the active site and two regions that we predict are in the proximity of the active site. This conclusion is supported by a surface view of the SEX4 DSP domain model (Figure 9C). This view demonstrates that these regions envelop the active site (shown in red) and are concentrated around the active site.

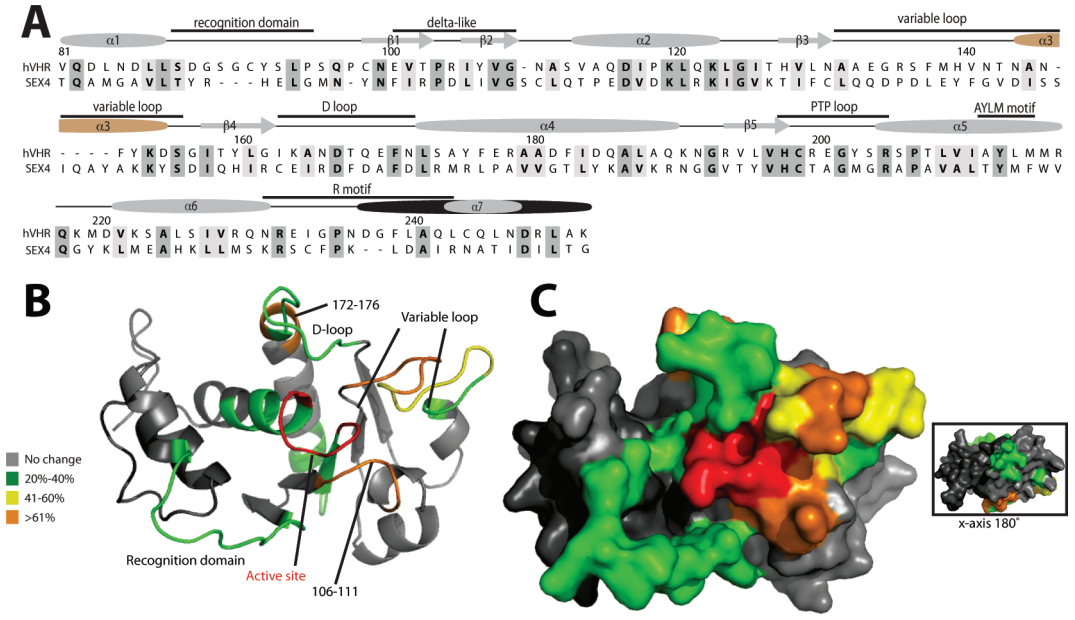

FIGURE 9: DSP domain decreases in percent deuteration upon amylopectin binding. (A) Alignment of the DSP domain of human VHR (hVHR) and SEX4. Above the amino acids is a comparison between the predicted secondary structures of the SEX4 DSP domain with the known secondary structure of VHR. The α-helices and *β*-sheets are numbered per accepted DSP domain nomenclature (*59*). Gray α-helices and *β*-sheets represent common structural features between hVHR and SEX4; the tan α-helix 3 represents a structural feature lacking in hVHR but present in SEX4 and in most DSP domains, and the black α-helix 7 represents an extended helix of hVHR compared to the gray predicted helix of SEX4. Numbers above the amino acids refer to their position in full-length SEX4. (B) Ribbon structure of the SEX4 DSP domain model with the percent change in deuteration from Figure 8 mapped onto it. The active site is highlighted in red, and the percent change corresponds to the inset. The DSP regions of interest are also labeled. (C) Surface view of the SEX4 DSP domain model with the percent change in deuteration mapped onto it. Percent change colors are as in panel B. The inset is a view of the surface after the model has been rotated 180° on the *x*-axis. The residues colored green in the center of this view are from peptide 184−209 covering the PTP-loop.

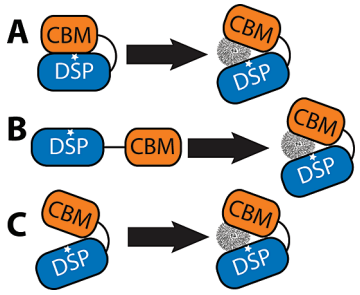

FIGURE 10: Schematic representing possible SEX4 dynamics. (A) In this model, the SEX4 CBM binds and precludes entry of the substrate into the DSP domain active site. Glucan binding triggers a substantial domain rearrangement that allows the active site to become available to the phosphoglucan. (B) Glucan binding by the CBM generates a global domain rearrangement that brings the glucan into contact with the DSP domain to allow phosphoglucan dephosphorylation. (C) The CBM binds the phosphoglucan and positions it appropriately so that the DSP comes into contact with the glucan. This binding results in minimal domain rearrangement and presents the phosphoglucan to the DSP domain active site.

The region demonstrating a decrease in the level of deuteration on the opposite face of the DSP domain corresponds to Tyr^{184}−Gly^{191} (Figure 9C, inset). The exchange data for these amino acids are on the same peptide as the PTP-loop, peptide 184−209 (Figure 3B). Thus, the resolution in this region is decreased compared with that of the majority of our data. We attempted to obtain peptides that separated the PTP-loop from these amino acids but were unable to do so. Nonetheless, we predict that residues 184−191 likely do not interact with the phosphoglucan and are highlighted due to the interaction between the PTP-loop residues and amylopectin.

DISCUSSION

To date, there have been no mechanistic or structural studies on the newly described glucan phosphatases. We utilized DXMS to determine how the two domains of one glucan phosphatase, SEX4, behave upon phosphoglucan binding. Our data suggest that SEX4 does not undergo a large-scale rearrangement upon glucan binding. Instead, our results suggest only minor rearrangement of the CBM and DSP domain upon glucan binding. Within the CBM, our data confirmed that peptides containing residues known to coordinate glucan binding perform a similar function in SEX4. While these results were as expected, the results we obtained concerning the DSP domain of SEX4 were quite insightful. These data identified regions within the SEX4 DSP domain and adjacent to the active site that intimately interact with the phosphoglucan, including the recognition domain, the D-loop, the variable loop, and the PTP-loop.

Changes that occur early in H−D exchange time course experiments are most often the result of differences in solvent accessibility caused by direct interaction of the peptide with the substrate and/or a conformational alteration in the protein upon substrate binding. Significant conformational alterations cause new residues to be exposed and others to be more protected, as is the case with Factor VIIa, Epac, the cytosolic group IVA phospholipase A_2, eIF4E, and ERK2 (*37*, *64*−*67*). Since Δ81-SEX4-C/S only undergoes weakened deuteration, the decreased level of deuteration occurs early in the experiment, and it lacks an increased level of deuteration, these data collectively argue that upon glucan binding there is no large-scale rearrangement of the CBM or DSP domain. It also suggests that there is not a subdomain conformational change that is then propagated throughout the domain or the protein, as this action would cause both increased and decreased levels of deuteration. Even upon

extending the time frame of our analysis by 100-fold, we observed only data suggestive of a local conformational change in one peptide, peptide 99−105 (data not shown). Instead, the data suggest that the regions undergoing weakened deuteration within both the CBM and DSP are being protected by the glucan itself.

Prior to this study, we envisioned three scenarios regarding the domain dynamics of the CBM and DSP domain of SEX4 (Figure 10). The first two scenarios, depicted in panels A and B of Figure 10, would each result in substantial domain rearrangement. Therefore, each of these cases would cause both an increase and decrease in the percent deuteration of the SEX4 CBM and DSP domain upon glucan binding. Since we did not observe an increase in the percent deuteration, our results indicate that SEX4 does not undergo a large-scale rearrangement upon glucan binding. Thus, our results suggest there is limited structural change in SEX4 upon glucan binding (Figure 10C) and eliminate models depicting global structural changes (Figure 10A,B).

Another major finding of this study is the result suggesting that the DSP domain itself makes extensive and intimate contact with the phosphoglucan. The extensive interaction between the DSP and amylopectin, and to a similar extent with β-cyclodextrin, is surprising, but not without some precedent. Myotubularin-related protein-2 (MTMR2) binds and dephosphorylates specific phosphoinositols (*60*, *68*−*71*). One region of the DSP domain of MTMR2 undergoes a similar 25% decrease upon binding phosphatidylinositol 3-phosphate in a region that forms an extension to the active site pocket (*68*). Multiple regions of the DSP domain of SEX4 interact with phosphoglucans in a similar manner as seen with the one region of MTMR2 and phosphoinositols, but the SEX4 DSP interacts with the phosphoglucan to a more extensive degree than was observed with MTMR2 and phosphatidylinositol 3-phosphate. The regions of the SEX4 DSP domain that interact with amylopectin are the recognition domain, the D-loop, the variable loop, the PTP-loop, peptide 106−111, and peptide 172−176. Our homology model predicts that each region is located on the same surface as the active site and that these regions engulf the SEX4 active site. Thus, they are located in a manner to interact with and present the phosphoglucan to the active site.

Our analyses also identified that the variable loop of SEX4 is atypical compared to other dual-specificity phosphatases (DSPs). The variable loop of most DSPs is shorter than the variable loop of protein tyrosine-specific phosphatases (PTPs). This difference is due to the need for a deeper active site in PTPs to accommodate the longer headgroup of a phospho-Tyr versus the shorter phospho-Ser/Thr. The deeper active site of PTPs largely accounts for their Tyr specificity, since P-Ser or P-Thr is essentially too short to reach the active site of PTPs. Interestingly, the variable loop of SEX4 is 25−50% longer than most DSPs, including the prototypical dual-specificity phosphatase VHR (Figure 9A). This increased length predicts that SEX4 likely has a deeper active site than DSPs that dephosphorylate phospho-proteinaceous substrates. Many of the DSPs that dephosphorylate nonproteinaceous substrates, e.g., PTEN and the myotubularins, have a deep and wide catalytic pocket to accommodate the phosphorylated inositol ring (*60*, *68*, *72*). Since SEX4 and laforin have a longer variable loop than dual-specificity phosphatases that act on proteinaceous substrates, we predict that the active site of glucan phosphatases will be deeper and wider than these phosphatases and more closely resemble that of phosphatases that dephosphorylate nonproteinaceous substrates.

In summary, our data support a model in which the DSP domain and CBM of SEX4 intimately interact with glucans and one in which the domains do not undergo global rearrangement upon glucan binding. The interactions between the SEX4 CBM and the glucan are as expected since carbohydrate binding modules by definition bind carbohydrates. However, the extensive interaction between the DSP domain and glucan is both surprising and insightful. Collectively, our results strengthen the case that SEX4 and, by inference, laforin are glucan phosphatases and provide the first structural insights into the dynamics of the CBM and DSP domain upon glucan binding.

ACKNOWLEDGMENT

We thank Drs. Craig Vander Kooi and Doug Andres for fruitful discussions regarding these data.

SUPPORTING INFORMATION AVAILABLE

A FPLC trace showing the gel-filtration purification of monomeric Δ81-SEX4-C198S (Figure S1), peptides within the dual-specificity phosphatase (DSP) domain that exhibit a $< 10\%$ change in the level of deuterium incorporation between apo and amylopectin-bound peptides (Figure S2), peptides outside of the DSP and CBM that exhibit a $< 10\%$ change in their level of deuterium incorporation (Figure S3), deuterium exchange results of apo and amylopectin-bound Δ81-SEX4 (Figure S4), and predicted secondary structure and domain topography of full-length SEX4 (Figure S5). This material is available free of charge via the Internet at http://pubs.acs.org.

REFERENCES

1. Hoof, F. V., and Hageman-Bal, M. (1967) Progressive familial myoclonic epilepsy with lafora bodies. *Acta Neuropathol. V7*, 315–326.
2. Lafora, G. R., and Gluck, B. (1911) Beitrag zur histopathologie der myoklonischen epilepsie. *Z. Gesamte Neurol. Psychiatr. 6*, 1–14.
3. Collins, G. H., Cowden, R. R., and Nevis, A. H. (1968) Myoclonus epilepsy with Lafora bodies. An ultrastructural and cytochemical study. *Arch. Pathol. 86*, 239–254.
4. Lafora, G. R. (1911) Uber des Vorkommen amyloider KJrperchen im innern der Ganglienzellen. *Virchows Arch. A: Pathol. Anat. 205*, 295.
5. Sakai, M., Austin, J., Witmer, F., and Trueb, L. (1970) Studies in myoclonus epilepsy (Lafora body form). II. Polyglucosans in the systemic deposits of myoclonus epilepsy and in corpora amylacea. *Neurology 20*, 160–176.
6. Yokoi, S., Austin, J., and Witmer, F. (1967) Isolation and characterization of Lafora bodies in two cases of myoclonus epilepsy. *J. Neuropathol. Exp. Neurol. 26*, 125–127.
7. Yokoi, S., Austin, J., Witmer, F., and Sakai, M. (1968) Studies in myoclonus epilepsy (Lafora body form). I. Isolation and preliminary characterization of Lafora bodies in two cases. *Arch. Neurol. 19*, 15–33.
8. Minassian, B. A., Lee, J. R., Herbrick, J. A., Huizenga, J., Soder, S., Mungall, A. J., Dunham, I., Gardner, R., Fong, C. Y., Carpenter, S., Jardim, L., Satishchandra, P., Andermann, E., Snead, O. C., III, Lopes-Cendes, I., Tsui, L. C., Delgado-Escueta, A. V., Rouleau, G. A., and Scherer, S. W. (1998) Mutations in a gene encoding a novel protein tyrosine phosphatase cause progressive myoclonus epilepsy. *Nat. Genet. 20*, 171–174.
9. Serratosa, J. M., Gomez-Garre, P., Gallardo, M. E., Anta, B., de Bernabe, D. B., Lindhout, D., Augustijn, P. B., Tassinari, C. A., Malafosse, R. M., Topcu, M., Grid, D., Dravet, C., Berkovic, S. F., and de Cordoba, S. R. (1999) A novel protein tyrosine phosphatase gene is mutated in progressive myoclonus epilepsy of the Lafora type (EPM2). *Hum. Mol. Genet. 8*, 345–352.
10. Wang, J., Stuckey, J. A., Wishart, M. J., and Dixon, J. E. (2002) A unique carbohydrate binding domain targets the lafora disease phosphatase to glycogen. *J. Biol. Chem. 277*, 2377–2380.

11. Gentry, M. S., Dowen, R. H., III, Worby, C. A., Mattoo, S., Ecker, J. R., and Dixon, J. E. (2007) The phosphatase laforin crosses evolutionary boundaries and links carbohydrate metabolism to neuronal disease. *J. Cell Biol. 178*, 477–488.
12. Worby, C. A., Gentry, M. S., and Dixon, J. E. (2006) Laforin: A dual specificity phosphatase that dephosphorylates complex carbohydrates. *J. Biol. Chem. 281*, 30412–30418.
13. Tagliabracci, V. S., Girard, J. M., Segvich, D., Meyer, C., Turnbull, J., Zhao, X., Minassian, B. A., Depaoli-Roach, A. A., and Roach, P. J. (2008) Abnormal metabolism of glycogen phosphate as a cause for lafora disease. *J. Biol. Chem. 283*, 33816–33825.
14. Tagliabracci, V. S., Turnbull, J., Wang, W., Girard, J. M., Zhao, X., Skurat, A. V., Delgado-Escueta, A. V., Minassian, B. A., Depaoli-Roach, A. A., and Roach, P. J. (2007) Laforin is a glycogen phosphatase, deficiency of which leads to elevated phosphorylation of glycogen in vivo. *Proc. Natl. Acad. Sci. U.S.A. 104*, 19262–19266.
15. Solaz-Fuster, M. C., Gimeno-Alcaniz, J. V., Ros, S., Fernandez-Sanchez, M. E., Garcia-Fojeda, B., Criado Garcia, O., Vilchez, D., Dominguez, J., Garcia-Rocha, M., Sanchez-Piris, M., Aguado, C., Knecht, E., Serratosa, J., Guinovart, J. J., Sanz, P., and Rodriguez de Cordoba, S. (2008) Regulation of glycogen synthesis by the laforin-malin complex is modulated by the AMP-activated protein kinase pathway. *Hum. Mol. Genet. 17*, 667–678.
16. Vilchez, D., Ros, S., Cifuentes, D., Pujadas, L., Valles, J., Garcia-Fojeda, B., Criado-Garcia, O., Fernandez-Sanchez, E., Medrano-Fernandez, I., Dominguez, J., Garcia-Rocha, M., Soriano, E., Rodriguez de Cordoba, S., and Guinovart, J. J. (2007) Mechanism suppressing glycogen synthesis in neurons and its demise in progressive myoclonus epilepsy. *Nat. Neurosci. 10*, 1407–1413.
17. Worby, C. A., Gentry, M. S., and Dixon, J. E. (2008) Malin decreases glycogen accumulation by promoting the degradation of protein targeting to glycogen (PTG). *J. Biol. Chem. 283*, 4069–4076.
18. Gentry, M. S., and Pace, R. M. (2009) Conservation of the glucan phosphatase laforin is linked to rates of molecular evolution and the glycogen metabolism of the organism. *BMC Evol. Biol. 9*, 138.
19. Niittyla, T., Comparot-Moss, S., Lue, W.-L., Messerli, G., Trevisan, M., Seymour, M. D. J., Gatehouse, J. A., Villadsen, D., Smith, S. M., Chen, J., Zeeman, S. C., and Smith, A. M. (2006) Similar protein phosphatases control starch metabolism in plants and glycogen metabolism in mammals. *J. Biol. Chem. 281*, 11815–11818.
20. Sokolov, L. N., Dominguez-Solis, J. R., Allary, A. L., Buchanan, B. B., and Luan, S. (2006) A redox-regulated chloroplast protein phosphatase binds to starch diurnally and functions in its accumulation. *Proc. Natl. Acad. Sci. U.S.A. 103*, 9732–9737.
21. Kerk, D., Conley, T. R., Rodriguez, F. A., Tran, H. T., Nimick, M., Muench, D. G., and Moorhead, G. B. (2006) A chloroplast-localized dual-specificity protein phosphatase in *Arabidopsis* contains a phylogenetically dispersed and ancient carbohydrate-binding domain, which binds the polysaccharide starch. *Plant J. 46*, 400–413.
22. Kotting, O., Santelia, D., Edner, C., Eicke, S., Marthaler, T., Gentry, M. S., Comparot-Moss, S., Chen, J., Smith, A. M., Steup, M., Ritte, G., and Zeeman, S. C. (2009) STARCH-EXCESS4 Is a Laforin-Like Phosphoglucan Phosphatase Required for Starch Degradation in *Arabidopsis thaliana*. *Plant Cell 21*, 334–346.
23. Smith, A. M., Zeeman, S. C., and Smith, S. M. (2005) Starch degradation. *Annu. Rev. Plant Biol. 56*, 73–98.
24. Zeeman, S. C., Smith, S. M., and Smith, A. M. (2007) The diurnal metabolism of leaf starch. *Biochem. J. 401*, 13–28.
25. Blennow, A., Nielsen, T. H., Baunsgaard, L., Mikkelsen, R., and Engelsen, S. B. (2002) Starch phosphorylation: A new front line in starch research. *Trends Plant Sci. 7*, 445–450.
26. Hejazi, M., Fettke, J., Haebel, S., Edner, C., Paris, O., Frohberg, C., Steup, M., and Ritte, G. (2008) Glucan, water dikinase phosphorylates crystalline maltodextrins and thereby initiates solubilization. *Plant J. 55*, 323–334.
27. Hvidt, A., and Nielsen, S. O. (1966) Hydrogen exchange in proteins. *Adv. Protein Chem. 21*, 287–386.
28. Linderstrom-Lang, K. U. (1958) Deuterium exchange and protein structure , Methuen, London.
29. Busenlehner, L. S., and Armstrong, R. N. (2005) Insights into enzyme structure and dynamics elucidated by amide H/D exchange mass spectrometry. *Arch. Biochem. Biophys. 433*, 34–46.
30. Hoofnagle, A. N., Resing, K. A., and Ahn, N. G. (2003) Protein analysis by hydrogen exchange mass spectrometry. *Annu. Rev. Biophys. Biomol. Struct. 32*, 1–25.
31. Tsutsui, Y., and Wintrode, P. L. (2007) Hydrogen/deuterium exchange-mass spectrometry: A powerful tool for probing protein structure, dynamics and interactions. *Curr. Med. Chem. 14*, 2344–2358.
32. Gentry, M. S., Worby, C. A., and Dixon, J. E. (2005) Insights into Lafora disease: Malin is an E3 ubiquitin ligase that ubiquitinates and promotes the degradation of laforin. *Proc. Natl. Acad. Sci. U.S.A. 102*, 8501–8506.
33. Burns-Hamuro, L. L., Hamuro, Y., Kim, J. S., Sigala, P., Fayos, R., Stranz, D. D., Jennings, P. A., Taylor, S. S., and Woods, V. L., Jr. (2005) Distinct interaction modes of an AKAP bound to two regulatory subunit isoforms of protein kinase A revealed by amide hydrogen/deuterium exchange. *Protein Sci. 14*, 2982–2992.
34. Hamuro, Y., Anand, G. S., Kim, J. S., Juliano, C., Stranz, D. D., Taylor, S. S., and Woods, V. L., Jr. (2004) Mapping intersubunit interactions of the regulatory subunit (RIα) in the type I holoenzyme of protein kinase A by amide hydrogen/deuterium exchange mass spectrometry (DXMS). *J. Mol. Biol. 340*, 1185–1196.
35. Pantazatos, D., Kim, J. S., Klock, H. E., Stevens, R. C., Wilson, I. A., Lesley, S. A., and Woods, V. L., Jr. (2004) Rapid refinement of crystallographic protein construct definition employing enhanced hydrogen/deuterium exchange MS. *Proc. Natl. Acad. Sci. U.S.A. 101*, 751–756.
36. Spraggon, G., Pantazatos, D., Klock, H. E., Wilson, I. A., Woods, V. L., Jr., and Lesley, S. A. (2004) On the use of DXMS to produce more crystallizable proteins: Structures of the *T. maritima* proteins TM0160 and TM1171. *Protein Sci. 13*, 3187–3199.
37. Brock, M., Fan, F., Mei, F. C., Li, S., Gessner, C., Woods, V. L., Jr., and Cheng, X. (2007) Conformational analysis of Epac activation using amide hydrogen/deuterium exchange mass spectrometry. *J. Biol. Chem. 282*, 32256–32263.
38. Zhang, Z., and Smith, D. L. (1993) Determination of amide hydrogen exchange by mass spectrometry: A new tool for protein structure elucidation. *Protein Sci. 2*, 522–531.
39. Soding, J. (2005) Protein homology detection by HMM-HMM comparison. *Bioinformatics 21*, 951–960.
40. Soding, J., Biegert, A., and Lupas, A. N. (2005) The HHpred interactive server for protein homology detection and structure prediction. *Nucleic Acids Res. 33*, W244–W248.
41. Zdobnov, E. M., and Apweiler, R. (2001) InterProScan: An integration platform for the signature-recognition methods in InterPro. *Bioinformatics 17*, 847–848.
42. Pei, J., Kim, B. H., and Grishin, N. V. (2008) PROMALS3D: A tool for multiple protein sequence and structure alignments. *Nucleic Acids Res. 36*, 2295–2300.
43. Arnold, K., Bordoli, L., Kopp, J., and Schwede, T. (2006) The SWISS-MODEL workspace: A web-based environment for protein structure homology modelling. *Bioinformatics 22*, 195–201.
44. Melo, F., Devos, D., Depiereux, E., and Feytmans, E. (1997) ANOLEA: A www server to assess protein structures. *Proc. Int. Conf. Intell. Syst. Mol. Biol., 5th,* 187–190.
45. Luthy, R., Bowie, J. U., and Eisenberg, D. (1992) Assessment of protein models with three-dimensional profiles. *Nature 356*, 83–85.
46. Christen, M., Hunenberger, P. H., Bakowies, D., Baron, R., Burgi, R., Geerke, D. P., Heinz, T. N., Kastenholz, M. A., Krautler, V., Oostenbrink, C., Peter, C., Trzesniak, D., and van Gunsteren, W. F. (2005) The GROMOS software for biomolecular simulation: GROMOS05. *J. Comput. Chem. 26*, 1719–1751.
47. Coutinho, P. M., and Henrissat, B. (1999) Carbohydrate-active enzymes: An integrated database approach. In Recent Advances in Carbohydrate Bioengineering (Gilbert, H. J., Davies, G. J., Henrissat, B., and Svensson, B., Eds.) pp 3−12, The Royal Society of Chemistry, Cambridge, U.K.
48. Machovic, M., and Janecek, S. (2006) Starch-binding domains in the post-genome era. *Cell. Mol. Life Sci. 63*, 2710–2724.
49. Cantarel, B. L., Coutinho, P. M., Rancurel, C., Bernard, T., Lombard, V., and Henrissat, B. (2009) The Carbohydrate-Active EnZymes database (CAZy): An expert resource for Glycogenomics. *Nucleic Acids Res. 37*, D233–D238.
50. Polekhina, G., Gupta, A., van Denderen, B. J., Feil, S. C., Kemp, B. E., Stapleton, D., and Parker, M. W. (2005) Structural basis for glycogen recognition by AMP-activated protein kinase. *Structure 13*, 1453–1462.
51. Denu, J. M., Stuckey, J. A., Saper, M. A., and Dixon, J. E. (1996) Form and Function in Protein Dephosphorylation. *Cell 87*, 361.
52. Yuvaniyama, J., Denu, J. M., Dixon, J. E., and Saper, M. A. (1996) Crystal structure of the dual specificity protein phosphatase VHR. *Science 272*, 1328–1331.
53. Polekhina, G., Gupta, A., Michell, B. J., van Denderen, B., Murthy, S., Feil, S. C., Jennings, I. G., Campbell, D. J., Witters, L. A., Parker, M. W., Kemp, B. E., and Stapleton, D. (2003) AMPK β subunit targets metabolic stress sensing to glycogen. *Curr. Biol. 13*, 867–871.

54. Zhou, B., Wu, L., Shen, K., Zhang, J., Lawrence, D. S., and Zhang, Z. Y. (2001) Multiple regions of MAP kinase phosphatase 3 are involved in its recognition and activation by ERK2. *J. Biol. Chem. 276*, 6506–6515.
55. Jia, Z., Barford, D., Flint, A. J., and Tonks, N. K. (1995) Structural basis for phosphotyrosine peptide recognition by protein tyrosine phosphatase 1B. *Science 268*, 1754–1758.
56. Wang, F., Li, W., Emmett, M. R., Hendrickson, C. L., Marshall, A. G., Zhang, Y. L., Wu, L., and Zhang, Z. Y. (1998) Conformational and dynamic changes of *Yersinia* protein tyrosine phosphatase induced by ligand binding and active site mutation and revealed by H/D exchange and electrospray ionization Fourier transform ion cyclotron resonance mass spectrometry. *Biochemistry 37*, 15289–15299.
57. Xie, L., Zhang, Y. L., and Zhang, Z. Y. (2002) Design and characterization of an improved protein tyrosine phosphatase substrate-trapping mutant. *Biochemistry 41*, 4032–4039.
58. Zhang, Y. L., Yao, Z. J., Sarmiento, M., Wu, L., Burke, T. R., Jr., and Zhang, Z. Y. (2000) Thermodynamic study of ligand binding to protein-tyrosine phosphatase 1B and its substrate-trapping mutants. *J. Biol. Chem. 275*, 34205–34212.
59. Alonso, A., Rojas, A., Godzik, A., and Mustelin, T. (2003) The dual-specific protein tyrosine phosphatase family , Vol. 5, Springer, Berlin.
60. Begley, M. J., and Dixon, J. E. (2005) The structure and regulation of myotubularin phosphatases. *Curr. Opin. Struct. Biol. 15*, 614–620.
61. Andersen, J. N., Mortensen, O. H., Peters, G. H., Drake, P. G., Iversen, L. F., Olsen, O. H., Jansen, P. G., Andersen, H. S., Tonks, N. K., and Moller, N. P. (2001) Structural and evolutionary relationships among protein tyrosine phosphatase domains. *Mol. Cell. Biol. 21*, 7117–7136.
62. Barford, D., Flint, A. J., and Tonks, N. K. (1994) Crystal structure of human protein tyrosine phosphatase 1B. *Science 263*, 1397–1404.
63. Stuckey, J. A., Schubert, H. L., Fauman, E. B., Zhang, Z. Y., Dixon, J. E., and Saper, M. A. (1994) Crystal structure of *Yersinia* protein tyrosine phosphatase at 2.5 Å and the complex with tungstate. *Nature 370*, 571–575.
64. Hsu, Y. H., Burke, J. E., Stephens, D. L., Deems, R. A., Li, S., Asmus, K. M., Woods, V. L., Jr., and Dennis, E. A. (2008) Calcium binding rigidifies the C2 domain and the intradomain interaction of GIVA phospholipase A2 as revealed by hydrogen/deuterium exchange mass spectrometry. *J. Biol. Chem. 283*, 9820–9827.
65. Rand, K. D., Andersen, M. D., Olsen, O. H., Jorgensen, T. J., Ostergaard, H., Jensen, O. N., Stennicke, H. R., and Persson, E. (2008) The origins of enhanced activity in factor VIIa analogs and the interplay between key allosteric sites revealed by hydrogen exchange mass spectrometry. *J. Biol. Chem. 283*, 13378–13387.
66. Zhou, B., Zhang, J., Liu, S., Reddy, S., Wang, F., and Zhang, Z. Y. (2006) Mapping ERK2-MKP3 binding interfaces by hydrogen/deuterium exchange mass spectrometry. *J. Biol. Chem. 281*, 38834–38844.
67. Rutkowska-Wlodarczyk, I., Stepinski, J., Dadlez, M., Darzynkiewicz, E., Stolarski, R., and Niedzwiecka, A. (2008) Structural changes of eIF4E upon binding to the mRNA 5′ monomethylguanosine and trimethylguanosine cap. *Biochemistry 47*, 2710–2720.
68. Begley, M. J., Taylor, G. S., Brock, M. A., Ghosh, P., Woods, V. L., and Dixon, J. E. (2006) Molecular basis for substrate recognition by MTMR2, a myotubularin family phosphoinositide phosphatase. *Proc. Natl. Acad. Sci. U.S.A. 103*, 927–932.
69. Begley, M. J., Taylor, G. S., Kim, S. A., Veine, D. M., Dixon, J. E., and Stuckey, J. A. (2003) Crystal structure of a phosphoinositide phosphatase, MTMR2: Insights into myotubular myopathy and Charcot-Marie-Tooth syndrome. *Mol. Cell 12*, 1391–1402.
70. Robinson, F. L., and Dixon, J. E. (2006) Myotubularin phosphatases: Policing 3-phosphoinositides. *Trends Cell Biol. 16*, 403–412.
71. Taylor, G. S., Maehama, T., and Dixon, J. E. (2000) Inaugural article: Myotubularin, a protein tyrosine phosphatase mutated in myotubular myopathy, dephosphorylates the lipid second messenger, phosphatidylinositol 3-phosphate. *Proc. Natl. Acad. Sci. U.S.A. 97*, 8910–8915.
72. Lee, J.-O., Yang, H., Georgescu, M.-M., Di Cristofano, A., Maehama, T., Shi, Y., Dixon, J. E., Pandolfi, P., and Pavletich, N. P. (1999) Crystal Structure of the PTEN Tumor Suppressor: Implications for Its Phosphoinositide Phosphatase Activity and Membrane Association. *Cell 99*, 323–334.